Characterization and Modelling of Tensile Flow Behavior of Ni Base Alloy 690 at Various Temperatures and Strain Rates

Jérôme Blaizot, Thibaut Chaise, Daniel Nelias, Michel Perez

CHARACTERIZATION AND MODELLING OF TENSILE FLOW BEHAVIOR OF NI BASE ALLOY 690 AT VARIOUS TEMPERATURES AND STRAIN RATES

Jérôme Blaizot
Université de Lyon, CNRS, INSA-Lyon, LaMCoS UMR5259
69621 Villeurbanne Cedex, France
Tel: +33(0)472437467
Email: jerome.blaizot@insa-lyon.fr

Thibaut Chaise
Université de Lyon, CNRS, INSA-Lyon, LaMCoS UMR5259
69621 Villeurbanne Cedex, France
Tel: +33(0)472436397
Email: thibaut.chaise@insa-lyon.fr

Daniel Nelias
Université de Lyon, CNRS, INSA-Lyon, LaMCoS UMR5259
69621 Villeurbanne Cedex, France
Tel: +33(0)472438490
Email: daniel.nelias@insa-lyon.fr

Michel Perez
Université de Lyon, CNRS, INSA-Lyon, MATEIS UMR5510
69621 Villeurbanne Cedex, France
Tel: +33(0)472438063
Email: michel.perez@insa-lyon.fr

ABSTRACT

Pressurized Water Reactor components are welded by Gas Tungsten Arc Welding (GTAW). To achieve good corrosion resistance and mechanical properties, Ni base alloy 690 is used to manufacture these components. The understanding of physical phenomena involved during welding and the prediction of induced residual stresses are crucial to guarantee high quality of these components. Welding induces drastic changes in the microstructure of the molten zone and heat-affected zone of metallic alloys especially for multi-pass welding. These changes may deteriorate the mechanical properties of the assembly. In order to reproduce the complex thermo-mechanical loading occurring within the heat affect zone, experiments on a thermo-mechanical simulator Gleeble 3500 have been carried out. In order to characterize the base alloy, isothermal tensile tests have been performed at various strain rates and temperatures (from 25 to 1100°C). A constitutive law has been proposed to predict the mechanical properties under different strain rates and temperatures. Tensile tests have also been performed after several thermal cycles to understand the effect of welding on mechanical properties of Ni alloy 690. In parallel, grain size evolution and carbide precipitation have been characterized and correlated to measured mechanical properties.

NOMENCLATURE

ρ	dislocation density
ε	true strain
$\dot{\varepsilon}$	strain rate
$\dot{\varepsilon}_0$	reference strain rate
σ	tensile true stress
σ_y	yield stress
ε_p	plastic strain
h	hardening parameter
r	dynamic recovery parameter
M	Taylor's constant
μ	shear modulus
b	magnitude of Burgers vector
Θ	strain hardening rate
Θ_0	initial strain hardening rate
σ_{ss}	saturation stress

INTRODUCTION

Pressurized Water Reactor components are welded by Gas Tungsten Arc Welding (GTAW). To achieve good corrosion resistance and mechanical properties, Ni base alloy 690 is used to manufacture these components. The understanding of physical phenomena involved during welding and the prediction of induced residual stresses are crucial to guarantee high quality of these components. Welding induces drastic changes in the microstructure of the molten zone and heat-affected zone of metallic alloys especially for multi-pass welding. These changes may deteriorate the mechanical properties of the assembly. In order to reproduce complex thermo-mechanical loading occurring within the heat affect zone, experiments on a thermo-mechanical simulator Gleeble 3500 have been conducted. In the present work, the Kocks-Mecking phenomenological approach is used to predict the stress-strain curves as a function of temperature and strain rate [**3-5**].

MATERIALS AND METHODS

The material chosen for this study is a nickel based superalloy namely alloy 690 used for Pressurized Water Reactor components of nuclear power plants. This alloy contains mainly nickel, chromium, iron and minor amounts of titanium, carbon and silicon. Like austenitic stainless alloys, this alloy contains carbides at grain boundaries in the austenite matrix.
Micrographic optic methods have been used to determine the initial grain size in the alloy and after tensile tests between 25 and 1000°C. The grain size and distribution have been determined by image analysis after an electrochemical etching at 2.5V during 20s in an electrolyte containing H_3PO_4, HNO_3 and H_2O. Characterization with a Scanning Electron Microscope has been performed to qualitatively quantify carbides at grain boundaries and to observe their morphologies. The composition of grain boundaries has been identified as $M_{23}C_6$ chromium carbides by using Transmission Electron Microscope. To reproduce complex thermo-mechanical loading occurring within the heat affected zone, tensile tests on the thermo-mechanical simulator Gleeble 3500 have been done from 25 to 1100 °C at various strain rates ranging from 10^{-4} to 5.10^{-3} s^{-1}. A constant deformation rate in the sample is imposed by using a longitudinal extensometer which operates up to 1100°C. The tensile tests were done on the alloy Ni 690 as received after the calibration of load cell and the hot extensometer. The measurement of Young's modulus was also confirmed by other method at 25°C.

EXPERIMENTAL RESULTS

Figures 1 and 2 show the initial microstructure and the morphology of grain boundary carbides in the initial material. Titanium nitrides are also present in the alloy and can be seen on figure 1. Grain boundary carbides have been identified as $M_{23}C_6$ carbides containing mainly chromium by using TEM. As pointed out by Li et al. [**1**], $M_{23}C_6$ carbides are partially coherent with the matrix.

Young's modulus has been determined between 25 and 1000°C and the values measured are similar to the technical data from Special Metals for alloy 690 [**2**] (fig. 3). Tensile yield strength has been also determined from 25 to 1100°C at a constant strain rate of 10^{-4} and $10^{-3}s^{-1}$ (fig. 4). Strain rate has an influence on yield stress above 900°C.

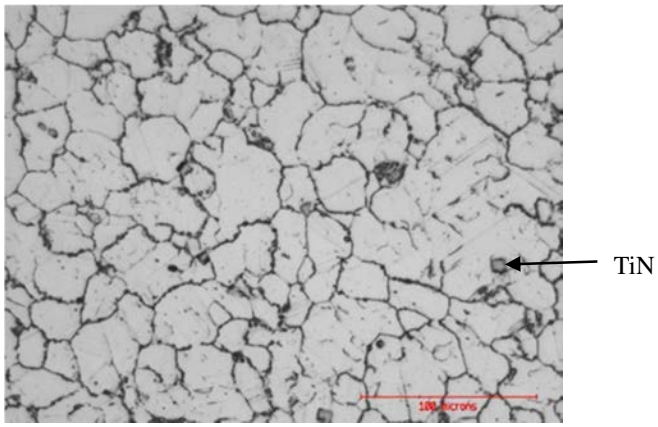

Fig. 1: optical image of the initial microstructure of alloy 690.

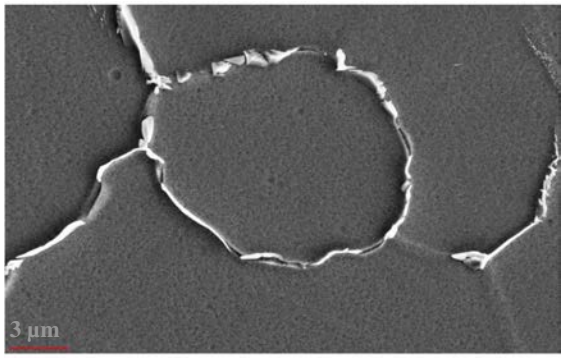

Fig. 2: SEM image of carbides at grain boundaries.

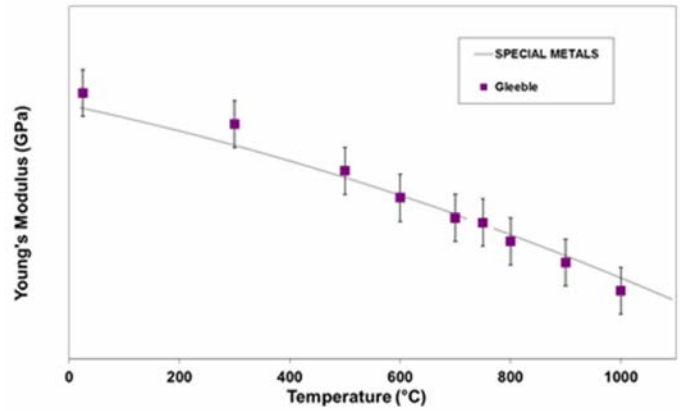

Fig. 3: evolution of Young's modulus versus temperature from 25 to 1000°C.

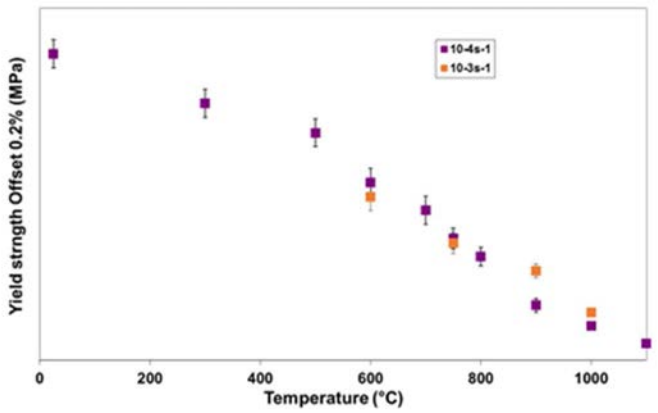

Fig. 4: evolution of Yield stress versus temperature at a strain rate of 10^{-4} and 10^{-3} s^{-1} from 25 to 1100°C.

From 25 to 600°C, strain hardening is predominant and a balance between strain hardening and dynamic recovery is observed above 750°C as illustrates on figure 5. A significant change of mechanical behavior occurs between 600 and 700°C. Strain hardening and stationary stress are greatly influenced by strain rate at 750°C (fig. 6).

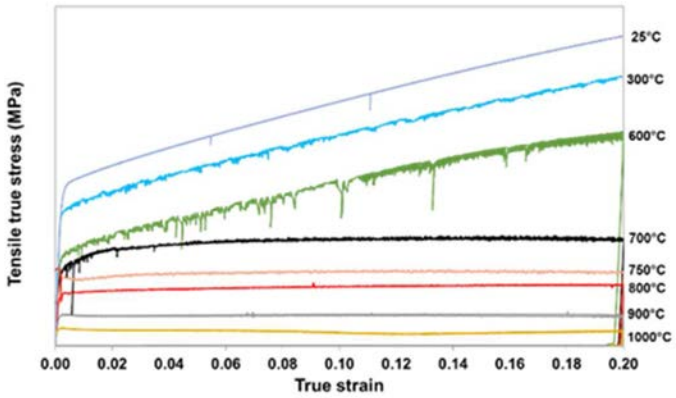

Fig. 5: stress-strain curves at a strain rate of $10^{-4}s^{-1}$ and various temperatures.

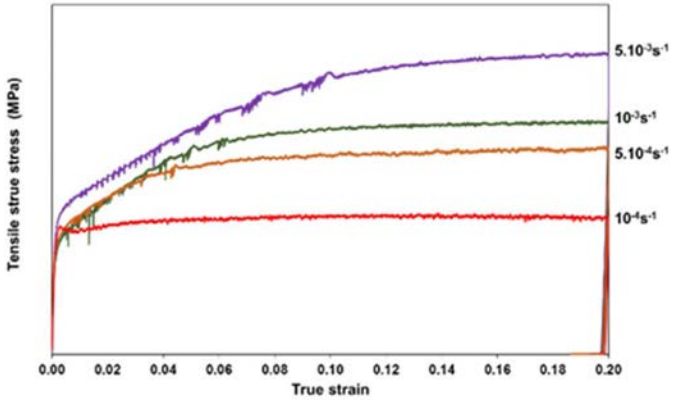

Fig. 6: stress-strain curves at a temperature of 750°C and various strain rates.

MODELLING OF MECHANICAL BEHAVIOR

Predicting the mechanical behavior as a function of strain rate and temperature requires the determination of yield stress, stationary stress and the evolution of hardening. To predict the yield stress from 25 to 1000°C with a unique law, an empiric relationship similar to Johnson-Cook can be used. Kocks-Mecking's model is particularly interesting to predict the isotropic strain hardening [**3-5**]. The Kocks-Mecking's model gives the evolution of the dislocation density ρ as follows:

$$\left|\frac{d\rho}{d\varepsilon}\right| = h\sqrt{\rho} - r\rho \qquad (1)$$

Parameters h and r are respectively the strain-hardening and dynamic recovery parameters.

Starting from this equation, the evolution of strain-hardening rate and flow stress can be determined by using Taylor's equation [**6**]:

$$\sigma = M\alpha\mu b\sqrt{\rho} \qquad (2)$$

By using equations (1) and (2), the evolution of strain-hardening rate Θ can be determined.

$$\Theta = \frac{d\sigma}{d\varepsilon} = \Theta_0\left(1 - \frac{\sigma}{\sigma_{ss}}\right) \qquad (3)$$

$$\text{where } \Theta_0 = \frac{M\alpha\mu b}{2} \text{ and } \sigma_{ss} = \frac{M\alpha\mu b}{r}$$

By integrating equation 1 and using equation 2, the macroscopic Voce's law is obtained.

$$\sigma = \sigma_{ss} - \left(\sigma_{ss} - \sigma_y\right) \times \exp\left(-\lambda\varepsilon_p\right) \qquad (4)$$

$$\text{where } \lambda = \frac{r}{2}$$

As shown on figures 5 and 6, the parameter r and the saturation stress σ_{ss} depend on temperature and strain rate [**7**]. The saturation stress is given by the following equation:

$$\sigma_{ss} = K\left(\frac{\dot{\varepsilon}}{\dot{\varepsilon}_0}\right)^m \exp\left(-\frac{Q}{RT}\right) \qquad (5)$$

In equation 5, K is a constant, Q the activation energy and m the strain rate sensitivity coefficient. The value of the reference strain rate $\dot{\varepsilon}_0$ is 10^{-4} s^{-1}. These coefficients have been calculated in two ranges of temperature: 25-600 and 600-1100°C.

For a temperature below 600°C, the hypothetic saturation stress is not a function of the strain rate. The activation energy is low and the hypothetic saturation stress decreases slowly as shown on figure 7.

The coefficient K and m of equation 5 have been also determined between 600 and 1100°C for a strain rate ranging from 10^{-4} to 5.10^{-3} s^{-1}. An activation energy Q of 68 kJ/mol has been found, this value is greatly lower than the activation energy of self-diffusion of nickel (219 kJ/mol) and vacancy migration (106 kJ/mol) [**8-9**]. The influence of temperature and strain rate on r in a large range of temperature is not clearly known. The

parameter r has been calculated between 25 and 750°C at various strain rates. Above 750°C, this parameter has not been calculated because the stress reaches the steady value σ_{ss} at the beginning of the plastic deformation. It dramatically increases from 600 to 700°C to reach a steady value for a strain rate of about 10^{-4} s^{-1}.

Finally, by predicting the yield stress, saturation stress and recovery parameter (fig. 7-8), the evolution of tensile stress can be calculated as function of temperature and strain rate (fig. 9-10). The challenge is to predict the change of mechanical behavior between 600 and 750°C by considering also the effect of strain rate on recovery parameter. The interest of this study is to keep the relative simplicity of Kocks-Mecking model which contains only one parameter that depends on temperature and strain rate.

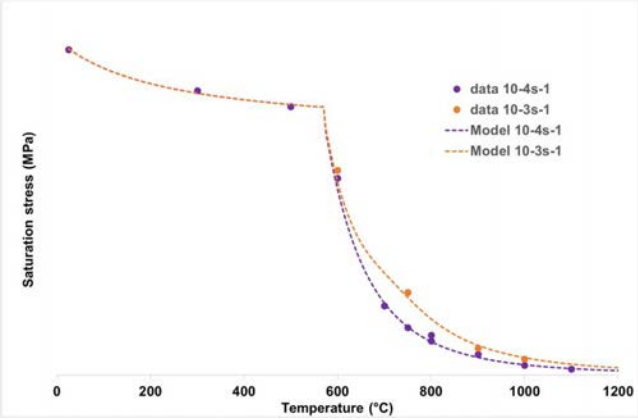

Fig. 7: experimental values and prediction of saturation stress versus temperature at various strain rates

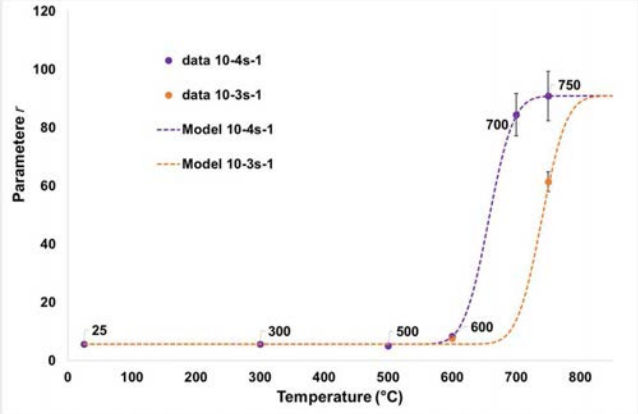

Fig. 8: experimental values and prediction of parameter r versus temperature at various strain rates.

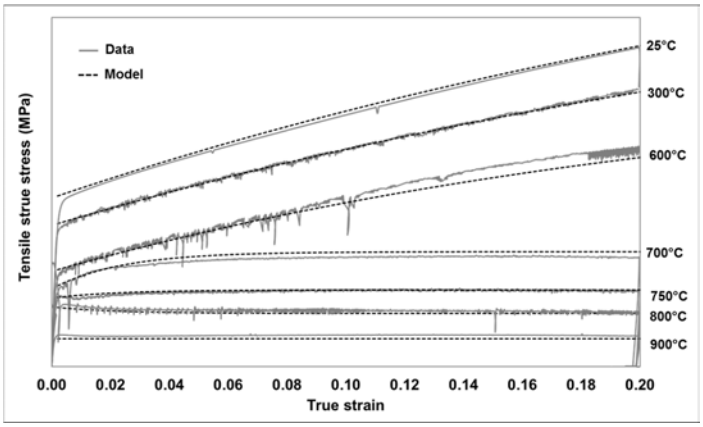

Fig. 9: prediction of the tensile stress at a constant strain rate of $10^{-4}s^{-1}$ and various temperatures and comparison with experimental data.

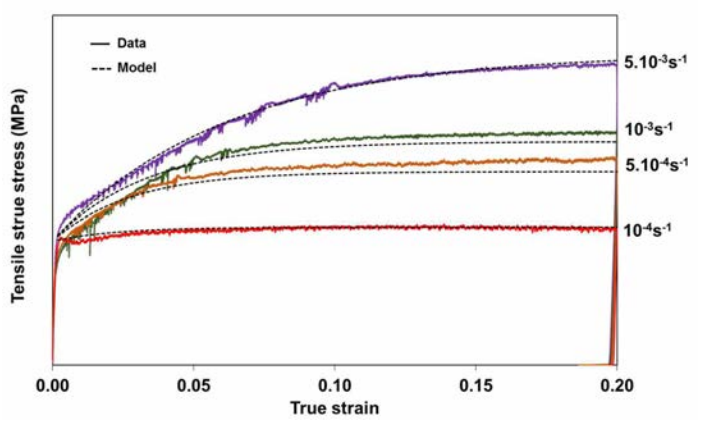

Fig. 10: prediction of the tensile stress at a temperature of 750°C and various strain rates and comparison with experimental data.

CONCLUSIONS

Tensile flow behavior has been studied between 25 and 1100°C at various strain rates including the effect of strain rate on strain hardening and dynamic recovery. By predicting the yield stress, saturation stress and recovery parameter depending on temperature and strain rate, the tensile stress has been calculated and the results are in a good agreement with the experimental data. Now, the prospects are to consider the effect of microstructure such as grain size on mechanical behavior and a better prediction of yield stress depending on temperature, strain rate and grain size. It also necessary to compare the results with independent data.

ACKNOWLEDGMENTS

The authors want to thank Philippe Gilles, Vincent Robin, Guillaume Tirand and Miguel Yescas (AREVA) and the AREVA-SAFRAN chair for supporting this research.

REFERENCES

[1] Li H *et al*. The growth mechanism of grain boundary carbide in alloy 690. *Materials Characterization* 81 (2013) 1-6.

[2] http://www.specialmetals.com/documents/Inconel%20alloy%20690.pdf

[3] Mecking H, Kocks UF. The kinetics of flow and strain hardening. *Acta Metallurgica* 29 (1981) 1865-1875.

[4] Estrin Y and Mecking H. A unified phenomenological description of wok hardening and creep based on one-parameter models. *Acta Metallurgica* 32 (1984) 57-70

[5] Kocks UF, Mecking H. Physics and phenomenology of strain hardening: the FCC case. *Progress in materials science 48* (2003) 171-273.

[6] Taylor GI. The mechanism of plastic deformation of crystals. Part I. Theoretical. *Proceedings of the Royal Society of London A*, 45:362–387, 1934.

[7] Sellars CM and McTeggart WJ. On the mechanism of hot deformation. *Acta Metallurgica* 14 (1966) 1136-1138.

[8] Walsöe De Reca E, Pampillo C. Self-diffusion of Ni in Ni-Fe alloys. *Acta Metallurgica* 15 (1967) 1263-1268.

[9] Chambron W, Caplain A. Etude des lacunes en très faible concentration dans l'alliage fer-nickel à 70% de nickel par la méthode de l'anisotropie magnétique. *Acta Metallurgica* 22 (1974) 357-366.